LETTER

Ultrastable silver nanoparticles

Anil Desireddy[1], Brian E. Conn[1], Jingshu Guo[1], Bokwon Yoon[2], Robert N. Barnett[2], Bradley M. Monahan[1], Kristin Kirschbaum[1], Wendell P. Griffith[1], Robert L. Whetten[3,4], Uzi Landman[2] & Terry P. Bigioni[1,5]

Noble-metal nanoparticles have had a substantial impact across a diverse range of fields, including catalysis[1], sensing[2], photochemistry[3], optoelectronics[4,5], energy conversion[6] and medicine[7]. Although silver has very desirable physical properties, good relative abundance and low cost, gold nanoparticles have been widely favoured owing to their proved stability and ease of use. Unlike gold, silver is notorious for its susceptibility to oxidation (tarnishing), which has limited the development of important silver-based nanomaterials. Despite two decades of synthetic efforts, silver nanoparticles that are inert or have long-term stability remain unrealized. Here we report a simple synthetic protocol for producing ultrastable silver nanoparticles, yielding a single-sized molecular product in very large quantities with quantitative yield and without the need for size sorting. The stability, purity and yield are substantially better than those for other metal nanoparticles, including gold, owing to an effective stabilization mechanism. The particular size and stoichiometry of the product were found to be insensitive to variations in synthesis parameters. The chemical stability and structural, electronic and optical properties can be understood using first-principles electronic structure theory based on an experimental single-crystal X-ray structure. Although several structures have been determined for protected gold nanoclusters[8–12], none has been reported so far for silver nanoparticles. The total structure of a thiolate-protected silver nanocluster reported here uncovers the unique structure of the silver thiolate protecting layer, consisting of Ag_2S_5 capping structures. The outstanding stability of the nanoparticle is attributed to a closed-shell 18-electron configuration with a large energy gap between the highest occupied molecular orbital and the lowest unoccupied molecular orbital, an ultrastable 32-silver-atom excavated-dodecahedral[13] core consisting of a hollow 12-silver-atom icosahedron encapsulated by a 20-silver-atom dodecahedron, and the choice of protective coordinating ligands. The straightforward synthesis of large quantities of pure molecular product promises to make this class of materials widely available for further research and technology development[14–18].

Silver thiolate clusters with an aromatic ligand shell and a core diameter of ~1.2 nm have been discovered only recently[19]. Electrospray-ionization mass spectrometry (ESI-MS) identified these as discrete molecular complexes, $Ag_{44}(SPh)_{30}^{4-}$, where SPh represents aryl thiolates[20]. Complexity of preparation and handling have proven limiting, however, as these clusters shared the typical vulnerabilities of Ag nanoparticles.

We have developed a new approach to the preparation of ultrastable silver nanoparticles in semiaqueous solution, which uses a protecting ligand shell of p-mercaptobenzoic acid (p-MBA)[8,19]. With judicious choice of solvent conditions and stabilizing agents, the fragile and unstable Ag complexes can be transformed into chemically inert materials with unprecedented stability. The synthesis involves the reduction of a soluble precursor in semiaqueous solution in the presence of alkali metal cations and a coordinating solvent. The straightforward protocol produces a pure molecular material without size separations and achieves near quantitative yield in large quantities (Fig. 1 inset). The product

can be dried and fully redispersed in protic, aprotic and nonpolar solvents with no loss of material or change in chemical identity.

The absorption spectrum of the raw product is highly structured (Fig. 1) and identical to that of the purified material, with an onset at about 1,100 nm (~1.1 eV). ESI-MS of the raw product (Fig. 2) identified several ion species that were all attributed to a single cluster size, the pure $Ag_{44}(p\text{-MBA})_{30}^{4-}$ complex (mass-to-charge ratio m/z 2,336). The $Ag_{43}(p\text{-MBA})_{28}^{3-}$ complex (m/z 2,975) was attributed to electrostatic destabilization and spontaneous fragmentation of $Ag_{44}(p\text{-MBA})_{30}^{4-}$ on desolvation (see Supplementary Information). The experimental data only matched the simulated isotopic distribution for the fully protonated species (see Supplementary Information), therefore the entire 4− charge was carried by the silver core rather than by the carboxylates. Four alkali counterions (M) were identified by elemental analysis, giving $M_4Ag_{44}(p\text{-MBA})_{30}$ as the molecular formula.

The synthesis of $M_4Ag_{44}(p\text{-MBA})_{30}$ has some characteristics not found in other nanoparticle preparations. Single-sized products are usually isolated by attrition: the less stable sizes are either destroyed or converted into the most stable size[21–23]. Direct synthesis of a truly single-sized molecular product with yields >95% indicates that these clusters are more stable than any other known cluster species. Furthermore, the particular size, composition and stoichiometry of the nanocluster product was found to be immune to changes in experimental parameters (for example, solvent composition, reactant concentrations) for the synthesis method reported here.

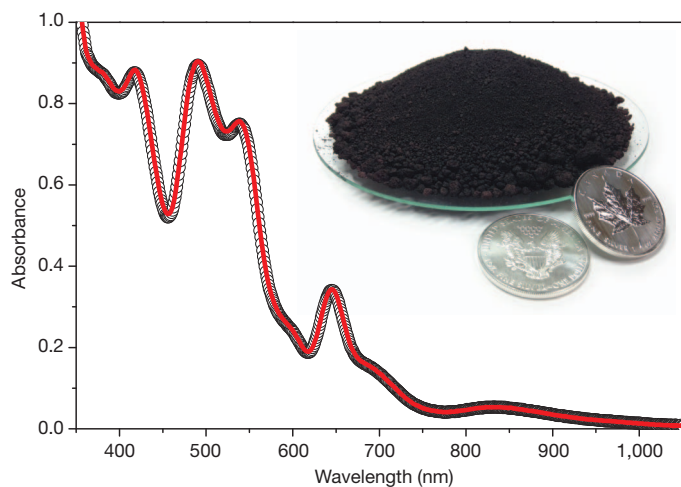The profound difference between canonical nanoparticle syntheses and the present work was demonstrated by synthesizing $M_4Ag_{44}(p\text{-MBA})_{30}$

Figure 1 | Optical absorption and material sample. Absorption spectrum of the $M_4Ag_{44}(p\text{-MBA})_{30}$ raw product solution (red line) synthesized in the presence of 'seed' $M_4Ag_{44}(p\text{-MBA})_{30}$ clusters (spectrum shown as open circles). Inset, 140 g of $M_4Ag_{44}(p\text{-MBA})_{30}$ clusters pictured with two one-ounce silver coins for scale (each coin is 4 cm in diameter and weighs 31.1 g). The dish is 18 cm in diameter.

[1]Department of Chemistry, University of Toledo, Toledo, Ohio 43606, USA. [2]School of Physics, Georgia Institute of Technology, Atlanta, Georgia 30332-0430, USA. [3]School of Chemistry and Biochemistry, Georgia Institute of Technology, Atlanta, Georgia 30332-0400, USA. [4]Department of Physics and Astronomy, University of Texas at San Antonio, San Antonio, Texas 78249, USA. [5]School of Solar and Advanced Renewable Energy, University of Toledo, Toledo, Ohio 43606, USA.
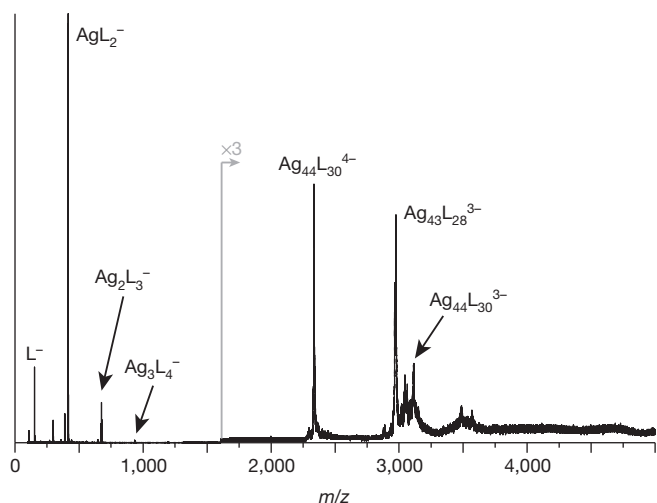
Figure 2 | Electrospray-ionization mass spectrum. ESI-MS of the final product without size separation shows that only one species is present. Peaks from 3,000–3,200 m/z are fragments with 3− charge state, and the broad intensity at 3,500 m/z is attributed to non-specific dimerization of fragments with 5− total charge state (see Supplementary Information for further details). Here, L is p-MBA.

clusters in the presence of existing $M_4Ag_{44}(p$-MBA$)_{30}$ clusters. Normally the existing nanoparticles would act as seeds and grow at the expense of new particle nucleation[24]. Instead, $M_4Ag_{44}(p$-MBA$)_{30}$ clusters were formed with identical yield and chemical identity, with or without these seeds present (Fig. 1). Once formed, $M_4Ag_{44}(p$-MBA$)_{30}$ clusters were very stable and unreactive, behaving as inert molecules rather than as typical nanoparticles. When an analogous reaction was performed with $Au_{25}(SG)_{18}$ (SG = glutathionate), the clusters were not inert but rather acted as canonical seeds (see Supplementary Information).

The long-term stability of solutions of $M_4Ag_{44}(p$-MBA$)_{30}$ clusters were also superior to those of $Au_{25}(SG)_{18}$ clusters. The ambient decay rates of $M_4Ag_{44}(p$-MBA$)_{30}$ cluster solutions were ∼7 times slower than those of $Au_{25}(SG)_{18}$ cluster solutions (see details in Supplementary Information and Supplementary Fig. 4b). Therefore, under both ambient (mildly oxidizing) and reducing conditions, the $M_4Ag_{44}(p$-MBA$)_{30}$ clusters proved to be more noble than even the highly stable $Au_{25}(SG)_{18}$ cluster[21]. When discussing relative stabilities of protected nanoclusters, caution should be exercised with regard to the ligands used and the environmental conditions (see Supplementary Information). Indeed, experiments in our laboratory have shown that $Au_{25}(p$-MBA$)_{18}$ clusters are too unstable for meaningful temporal stability measurements to be made.

This inertness under reducing conditions implies that the synthesis of new clusters can carry on without regard for existing clusters in the reaction vessel, giving impetus to scaling up the reaction. Indeed, it has been possible to produce 140 g of the final $M_4Ag_{44}(p$-MBA$)_{30}$ product from a single reaction (Fig. 1 inset), although kilogram-scale syntheses should be easily achievable. We note that 140 g is three orders of magnitude larger than typical nanoparticle preparations.

Clues as to the origins of the stability of $M_4Ag_{44}(p$-MBA$)_{30}$ as well as the structure of the thiol surface layers that protect the silver nanoparticles have been revealed by single-crystal X-ray diffraction. $Na_4Ag_{44}(p$-MBA$)_{30}$ clusters were crystallized from dimethylformamide (DMF) solution, with rhombus-shaped crystals forming after 1–3 days. The entire structure of the cluster was determined by single-crystal X-ray crystallography (see Supplementary Information), and is shown in Fig. 3a, b.

The crystal structure has exceptionally high symmetry, containing elements that exhibit four of the five Platonic solids. The all-silver core consists of a hollow icosahedron (Ag_{12} inner core) within a dodecahedron (Ag_{20} outer core), forming an Ag_{32} excavated-dodecahedral
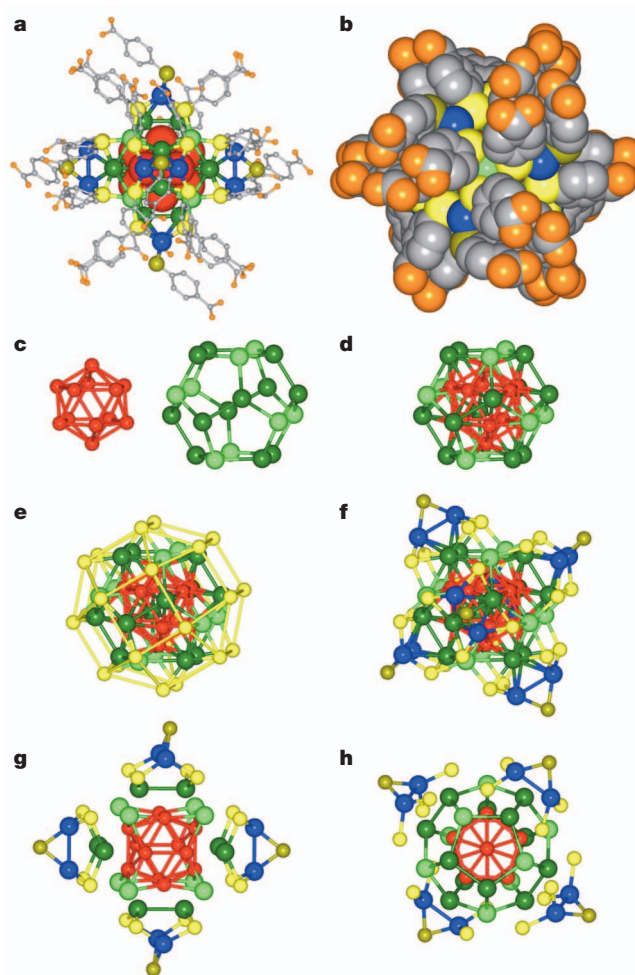

Figure 3 | X-ray crystal structure obtained from a $Na_4Ag_{44}(p$-MBA$)_{30}$ crystal. a, Complete cluster structure showing silver core and p-MBA ligands (see colour scheme below). **b**, Space-filling view down a three-fold axis (see colour scheme below). Note face-to-face and edge-to-face π stacking in the groupings of two and three ligands, resulting in considerable void space. **c**, The Ag_{32} excavated-dodecahedral core consists of an inner 12-atom (hollow) icosahedron (red) whose atoms do not contact sulphur, encapsulated by a 20-atom dodecahedron (green). **d**, The complete Ag_{32} excavated-dodecahedral core. The eight atoms of the dodecahedron that are coloured light green define a cube, with pairs of dark-green Ag atoms located above the faces. **e**, Sulphur atoms (yellow) are arranged in a slightly distorted rhombicuboctahedron with S atoms in the triangular faces coordinating to the light-green Ag atoms of the 20-atom dodecahedron. **f**, Six faces of the rhombicuboctahedron are capped with an Ag_2S unit with the bridging S atom tilted off axis, completing the inorganic structure (see colour scheme below). **g**, Two Ag atoms (dark green) on each face could be excised from the cluster to create Ag_4S_5 capping mount structures, leaving a cubic $Ag_{20}{}^{2+}$ core. The distance between the two Ag atoms at the bottom of the mount and the nearest Ag atoms of the Ag_{20} core is 2.83 Å, resulting in strong mount-to-core coupling. **h**, An alternative Ag_2S_5 capping structure can be visualized as a sawhorse-shaped mount that straddles the dark-green Ag atoms of the intact dodecahedral Ag_{32} core. The Ag_2S_5 mount is better defined than the Ag_4S_5 mount (see **g**) because its Ag atoms are separated by a larger distance (>3.1 Å) from the nearest atoms of the Ag_{32} core, resulting in a weaker mount-to-core interaction. Colour scheme: grey, carbon; orange, oxygen; blue, exterior silver atoms in the mounts; gold, bridging sulphur atoms in the mounts. For interatomic distances, see Supplementary Information.

core with icosahedral symmetry (Fig. 3c, d) whose compact geometric shape contributes to the cluster stability; interestingly, a hollow core has been recently put forward theoretically for another thiol-protected Ag cluster[25]. The 20 atoms of the outer core occupy two distinct environments. Eight Ag atoms within the dodecahedral outer core define the vertices of a cube (light green in Fig. 3), the faces of which contain

the remaining 12 Ag atoms in pairs (dark green in Fig. 3) and are capped in such a way as to create an overall octahedral shape for the particle (Fig. 3f). Namely, four sulphur atoms from the p-MBA ligands are located on each face of the cube, such that the 24 sulphurs define a slightly distorted rhombicuboctahedron, an Archimedean solid (Fig. 3e). Each face then receives an additional Ag_2S group to complete the inorganic part of the structure and the octahedral shape.

The capping units are complex three-dimensional structures unlike anything seen in gold clusters (one-dimensional gold-thiolate chains)[8–12] or in silver thiolate materials (two-dimensional silver-thiolate sheets)[26]. They can be viewed most simply as Ag_2S_5 'mounts', with four S atoms acting as legs that connect it to the Ag_{32} core. (We borrow the term 'mount' from the decorative arts, where it refers to a three-dimensional decoration added to an object.) These four S atoms are bridged by a pair of Ag atoms, which are in turn bridged by a terminal S atom. Each sawhorse-shaped mount straddles a pair of Ag atoms (dark green in Fig. 3) of the intact Ag_{32} core. Altogether, six such Ag_2S_5 mounts comprise the entire layer protecting the compact, quasi-spherical Ag_{32} core. The two relatively exposed Ag atoms[27] on each side of the six mounts can acquire effective protection from the coordinating solvent, consistent with experimental observations. If this protection is lost, the clusters can polymerize to form larger plasmonic Ag nanoparticles.

Further insight into the bonding and electronic structure of the $Ag_{44}(p\text{-MBA})_{30}{}^{4-}$ cluster was gained through extensive first-principles calculations[27]. Figure 4 shows the projected densities of states (PDOS, see Supplementary Information for details) calculated via density functional theory (DFT) based on the experimental configuration of the entire cluster (Fig. 3a); the PDOS reflects the angular momenta (l) symmetries of the cluster's orbitals[28], denoted as S, P, D,

F...(corresponding to $l = 0, 1, 2, 3,...$). The first outstanding feature observed is the relatively large energy gap between the highest occupied (HOMO) and the lowest unoccupied (LUMO) molecular orbitals, $\Delta_{HL} = 0.78$ eV, conferring stability on the cluster and endowing it with resistance to chemical attack. The first calculated optically allowed transition occurs at 0.98 eV, however, from the 1D HOMO (here, '1' is the principal quantum number) to the 1F LUMO+1 orbital, in fair agreement with the measured onset of optical absorption (≤ 1.1 eV, see Fig. 1).

The wavefunctions of the cluster exhibit both localized and delocalized character. The localized states are derived from the atomic Ag $4d$ electrons and are located at the middle of the energy spectrum, whereas the delocalized states are derived from the atomic Ag $5s$ electrons and can be found near the top and bottom of the electronic spectrum[28]. These delocalized cluster states can be assigned angular momentum symmetries following the electronic cluster shell model[28–30], with a (superatom) Aufbau rule: $1S^2 | 1P^6 | 1D^{10} | 2S^2 | 1F^{14} |....$ Here, the vertical lines denote shell-closures, which are associated with magic numbers: that is, closed-shell electronic structures are accompanied by the opening of a stabilizing energy gap. The number of electrons not engaged in bonding to sulphur (thiolates) is given by the electron count $n^* = vN_{Ag} - N_L - Z$, where $v = 1$ is the valence for Ag ($5s^1$), N_{Ag} is the number of Ag atoms, N_L is the number of anionic thiolate ligands, and Z is the overall cluster charge. For the case of $Ag_{44}(p\text{-MBA})_{30}{}^{4-}$, the electron count is $n^* = 18$, which corresponds to the stable superatom with the Aufbau shell filling $1S^2 | 1P^6 | 1D^{10} |$.

The 18-electron superatom shell-closure and accompanying energy gap stabilization enables a deeper insight into the structure of the protective silver-thiolate layer. Two alternative motifs for the aforementioned capping-ligand mounts can be constructed, as shown in
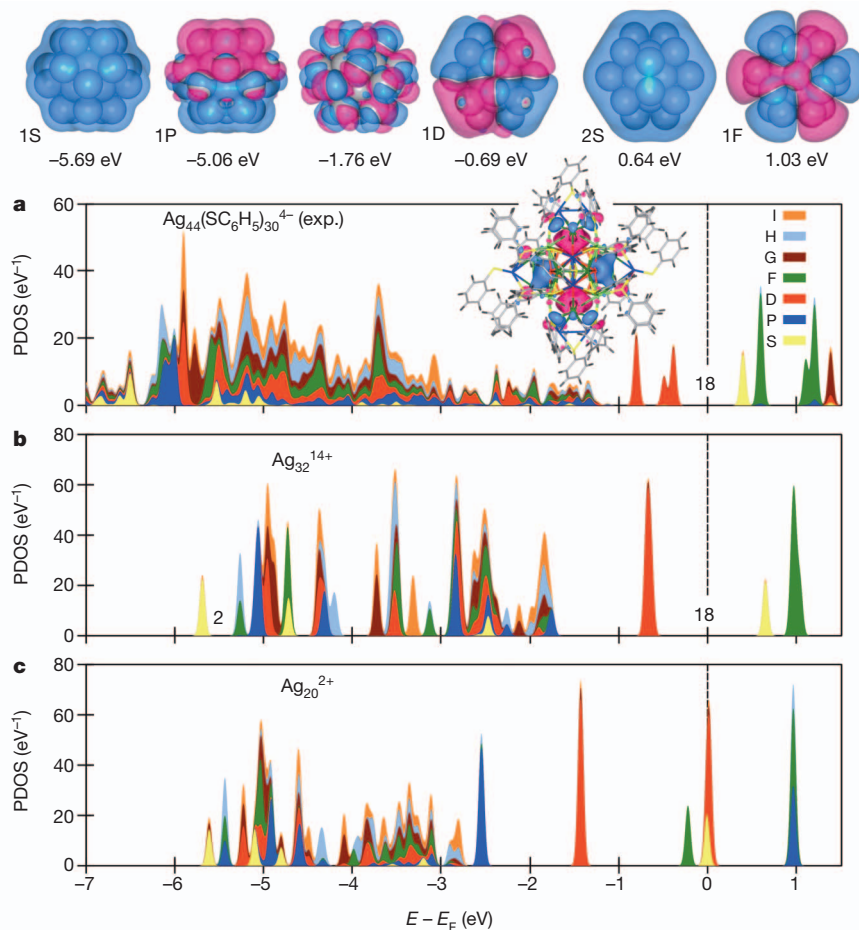

Figure 4 | Projected densities of states and orbital images. a, Potential densities of states (PDOS) calculated for the $Ag_{44}(SC_6H_5)_{30}{}^{4-}$ cluster with all atoms at the X-ray determined positions (see Methods and Supplementary Information). Different colours correspond to the various angular momentum contributions S, P, D, F, G, H and I, as shown on the right. The Fermi energy E_F is the energy in the middle of the HOMO–LUMO gap, $\Delta_{HL} = 0.78$ eV. The inset shows an image of the HOMO one-dimensional superatom orbital superimposed on the structure of the cluster; different colours of the orbital (blue and pink) corresponding to different signs of the wavefunction. The 18-electron gap is marked. **b**, PDOS of the $Ag_{32}{}^{14+}$ core, as extracted from the measured structure, corresponding to the $Ag_2S_5{}^{3-}$ mount motif. Selected superatom orbitals are shown at the top of the figure, with the energies and angular momenta marked. The 18-electron gap $\Delta_{HL} = 1.29$ eV is noted. **c**, PDOS of the $Ag_{20}{}^{2+}$ core, as extracted from the measured structure, corresponding to the $Ag_4S_5{}^-$ mount motif. Note the absence of an 18-electron gap.

Fig. 3. The cluster can be decomposed into six $Ag_4(p\text{-}MBA)_5^-$ mount units and a cubic Ag_{20}^{2+} core (Fig. 3g), where the formal charges result from the valences assigned to the silver atoms (1+) and p-MBA (thiolate) ligands (1−). Alternatively, the cluster can be decomposed into six $Ag_2(p\text{-}MBA)_5^{3-}$ mounts and a quasi-spherical Ag_{32}^{14+} core (Fig. 3h). In both cases, the cluster cores contain 18 Ag 5s electrons.

Electronic structure calculations on the two proposed cores, as extracted from the X-ray determined structure, provide a way to differentiate these two competing motifs. The PDOS of the Ag_{32}^{14+} cluster core (Fig. 4b) bears a great similarity to that of the entire cluster, including a large HOMO–LUMO gap (Fig. 4a) and a marked degeneracy of the $1D^{10}$ superatom orbitals, reflecting an approximate spherical symmetry of the effective potential governing the motion of the delocalized electrons of the cluster core (the corresponding superatom orbital shapes are shown at the top of Fig. 4). In contrast, similar analysis for the Ag_{20}^{2+} cluster core results in a spectrum that differs considerably from that of the complete particle, and in particular does not exhibit a gap (Fig. 4c), reflecting strong coupling of this core to the $Ag_4(p\text{-}MBA)_5$ mounts. The $Ag_2(p\text{-}MBA)_5$ mounts can therefore be thought of as the operative capping unit and Ag_{32} as the natural choice for the core.

METHODS SUMMARY

Synthetic methods. $M_4Ag_{44}(p\text{-}MBA)_{30}$ clusters are prepared in essentially quantitative yield by a simple three-step procedure: (1) generation of a $Ag(\textsc{i})\text{-}p\text{-}MBA$ precursor; (2) reduction of the precursor to the product; and (3) removal of by-products. Afterward, the pure substance is protonated.

(1) Aqueous $AgNO_3$ is combined with ethanolic p-MBA in excess to form the insoluble $Ag(\textsc{i})\text{-}p\text{-}MBA$ precursor. The pH is then adjusted to 9 with CsOH to solubilize the precursor and is further adjusted to 12 to stabilize the final cluster product. (2) Aqueous $NaBH_4$ is then added dropwise with stirring and is allowed to incubate for an hour. The final dark red solution yields the $M_4Ag_{44}(p\text{-}MBA)_{30}$ product with the carboxylates as alkali metal salts. (3) The clusters are separated from the reaction mixture by precipitation with DMF. The carboxylates are then protonated with acetic acid until the cluster completely dissolves in DMF, yielding the stoichiometric $M_4Ag_{44}(p\text{-}MBA)_{30}$ final product, which is isolated by precipitation.

X-ray crystallography. Data were collected for an $80\,\mu m \times 70\,\mu m \times 50\,\mu m$ crystal at 150 K with a Bruker Apex Duo diffractometer (CuKα = 1.54178 Å) equipped with an APEX II CCD detector. The structure was solved and refined using the Bruker SHELXTL software package, with space group $R\bar{3}c$. All eight crystallographically independent Ag atoms were obtained by direct methods and all remaining non-hydrogen atoms were located with subsequent difference Fourier techniques. The refinement converged to $R_1 = 5.2\%$ with a maximum resolution of 0.83 Å. The highest residual electron density was $1.036\,e\,\text{Å}^{-3}$.

Computational methods. The VASP-DFT package was used, with a plane-wave basis, kinetic energy cut-off of 400 eV, PAW pseudopotentials[31], and the PW91 generalized gradient approximation for exchange-correlation[32,33]. In structural optimizations, convergence was achieved for forces $<0.001\,\text{eV}\,\text{Å}^{-1}$. Calculations were performed for the X-ray determined $Ag_{44}(SC_6H_5)_{30}^{4-}$ structure (hydrogens were added and their positions were relaxed, average $d(\text{C–H}) = 1.09\,\text{Å}$).

1. Heiz, U. & Landman, U. (eds) *Nanocatalysis* (Springer, 2007).
2. Anker, J. N. et al. Biosensing with plasmonic nanosensors. *Nature Mater.* **7,** 442–453 (2008).
3. Jin, R. et al. Controlling anisotropic nanoparticle growth through plasmon excitation. *Nature* **425,** 487–490 (2003).
4. Maier, S. A. et al. Plasmonics — a route to nanoscale optical devices. *Adv. Mater.* **13,** 1501–1505 (2001).
5. Noginov, M. A. et al. Demonstration of a spaser-based nanolaser. *Nature* **460,** 1110–1112 (2009).
6. Atwater, H. A. & Polman, A. Plasmonics for improved photovoltaic devices. *Nature Mater.* **9,** 205–213 (2010).
7. Arvizo, R. R. et al. Intrinsic therapeutic applications of noble metal nanoparticles: past, present and future. *Chem. Soc. Rev.* **41,** 2943–2970 (2012).
8. Jadzinsky, P. D., Calero, G., Ackerson, C. J., Bushnell, D. A. & Kornberg, R. D. Structure of a thiol monolayer-protected gold nanoparticle at 1.1 Å resolution. *Science* **318,** 430–433 (2007).
9. Heaven, M. W., Dass, A., White, P. S., Holt, K. M. & Murray, R. W. Crystal structure of the gold nanoparticle [N(C₈H₁₇)₄][Au₂₅(SCH₂CH₂Ph)₁₈]. *J. Am. Chem. Soc.* **130,** 3754–3755 (2008).
10. Zhu, M., Aikens, C. M., Hollander, F. J., Schatz, G. C. & Jin, R. Correlating the crystal structure of a thiol-protected Au₂₅ cluster and optical properties. *J. Am. Chem. Soc.* **130,** 5883–5885 (2008).
11. Qian, H., Eckenhoff, W. T., Zhu, Y., Pintauer, T. & Jin, R. Total structure determination of thiolate-protected Au₃₈ nanoparticles. *J. Am. Chem. Soc.* **132,** 8280–8281 (2010).
12. Zeng, C. et al. Total structure of the golden nanocrystal Au₃₆(SR)₂₄. *Angew. Chem. Int. Edn* **51,** 13114–13118 (2012).
13. Williams, R. *The Geometrical Foundation of Natural Structure* (Dover, New York, 1979).
14. Krätschmer, W., Lamb, L. D., Fostiropoulos, K. & Huffman, D. R. Solid C₆₀: a new form of carbon. *Nature* **347,** 354–358 (1990).
15. Ebbesen, T. W. & Ajayan, P. M. Large-scale synthesis of carbon nanotubes. *Nature* **358,** 220–222 (1992).
16. Bethune, D. S. et al. Cobalt-catalysed growth of carbon nano-tubes with single-atomic-layer walls. *Nature* **363,** 605–607 (1993).
17. Murray, C. B., Norris, D. J. & Bawendi, M. G. Synthesis and characterization of nearly monodisperse CdE (E = S, Se, Te) semiconductor nanocrystallites. *J. Am. Chem. Soc.* **115,** 8706–8715 (1993).
18. Brust, M., Walker, M., Bethell, D., Schiffrin, D. J. & Whyman, R. Synthesis of thiol-derivatised gold nanoparticles in a two-phase liquid-liquid system. *J. Chem. Soc. Chem. Commun.* **1994,** 801–802 (1994).
19. Bakr, O. M. et al. Silver nanoparticles with broad multiband linear optical absorption. *Angew. Chem. Int. Edn* **48,** 5921–5926 (2009).
20. Harkness, K. M. et al. Ag₄₄(SR)₃₀⁴⁻: a silver–thiolate superatom complex. *Nanoscale* **4,** 4269–4274 (2012).
21. Shichibu, Y. et al. Extremely high stability of glutathione-protected Au₂₅ clusters against core etching. *Small* **3,** 835–839 (2007).
22. Cathcart, N. & Kitaev, V. Silver nanoclusters: single-stage scalable synthesis of mono-disperse species and their chiro-optical properties. *J. Phys. Chem. C* **114,** 16010–16017 (2010).
23. Dharmaratne, A. C., Krick, T. & Dass, A. Nanocluster size evolution studied by mass spectrometry in room temperature Au₂₅(SR)₁₈ synthesis. *J. Am. Chem. Soc.* **131,** 13604–13605 (2009).
24. Jana, N. R., Gearheart, L. & Murphy, C. J. Seeding growth for size control of 5−40 nm diameter gold nanoparticles. *Langmuir* **17,** 6782–6786 (2001).
25. Chakraborty, I. et al. The superstable 25-kDa monolayer protected silver nanoparticle: measurements and interpretation as an icosahedral Ag₁₅₂(SCH₂CH₂Ph)₆₀ cluster. *Nano Lett.* **12,** 5861–5866 (2012).
26. Dance, I. G. The structural chemistry of metal thiolate complexes. *Polyhedron* **5,** 1037–1104 (1986).
27. Herron, N., Calabrese, J. C., Farneth, W. E. & Wang, Y. Crystal structure and optical properties of Cd₃₂S₁₄(SC₆H₅)₃₆•DMF₄, a cluster with a 15 Å CdS core. *Science* **259,** 1426–1428 (1993).
28. Yoon, B. et al. Size-dependent structural evolution and chemical reactivity of gold clusters. *ChemPhysChem* **8,** 157–161 (2007).
29. Knight, W. D. et al. Electronic shell structure and abundances of sodium clusters. *Phys. Rev. Lett.* **52,** 2141–2143 (1984).
30. Yannouleas, C. & Landman, U. in *Recent Progress in Orbital-Free Density Functional Theory* (eds Wesolowski, T. A. & Wang, Y. A.) 203–250 (World Scientific, 2013).
31. Kresse, G. & Joubert, D. From ultrasoft pseudopotentials to the projector augmented-wave method. *Phys. Rev. B* **59,** 1758–1775 (1999).
32. Perdew, J. P. in *Electronic Structure of Solids '91* (eds Ziesche, P. & Eschrig, H.) 11–20 (Akademie, 1991).
33. Perdew, J. P. et al. Atoms, molecules, solids, and surfaces: applications of the generalized gradient approximation for exchange and correlation. *Phys. Rev. B* **46,** 6671–6687 (1992); Erratum. *Phys. Rev. B* **48,** 4978–4978 (1993).

Author Contributions T.P.B. conceived, directed and analysed all experimental research except for mass spectrometry, which W.P.G. directed and analysed, and X-ray diffraction, which K.K. directed and analysed. A.D., B.E.C. and B.M.M. performed all experimental work except for mass spectrometry, which J.G. performed. All computations and theoretical analyses were done by B.Y., R.N.B. and U.L. All authors contributed to the preparation of the manuscript.

Author Information The X-ray crystallographic coordinates have been deposited in the Cambridge Crystallographic Data Centre with CCDC number 949240. Reprints and permissions information is available at www.nature.com/reprints. The authors declare no competing financial interests. Readers are welcome to comment on the online version of the paper. Correspondence and requests for materials should be addressed to T.P.B. (Terry.Bigioni@utoledo.edu).